

# An upper bound to gas storage and delivery via pressure-swing adsorption in porous materials

Jordan Pommerenck and David Roundy

*Department of Physics, Oregon State University, Corvallis, OR 97331*

Cory Simon

*Department of Chemical Engineering, Oregon State University, Corvallis, OR 97331*

Both hydrogen and natural gas are challenging to economically store onboard vehicles as fuels, due to their low volumetric energy density at ambient conditions. One strategy to densify these gases is to pack the fuel tank with a porous adsorbent material. The US Department of Energy (DOE) has set volumetric deliverable capacity targets which, if met, would help enable commercial adoption of hydrogen/natural gas as transportation fuels. Here, we present a theoretical upper bound on the deliverable capacity of a gas in a rigid porous material via an isothermal pressure swing. To provide an extremum, we consider a substrate that provides a spatially uniform potential energy field for the gas. Our bound relies directly on experimentally measured properties of the pure gas. We conclude that the deliverable capacity targets set by the DOE for room-temperature natural gas and hydrogen storage are just barely theoretically possible. The targets are likely to be impossible for any real, rigid porous material because of steric repulsion, which reduces the deliverable capacity below our upper bound. Limitations to the scope of applicability of our upper bound may guide fuel tank design and future material development. Firstly, one could avoid using an *isothermal* pressure swing by heating the adsorbent to drive off trapped, residual gas. Secondly, our upper bound assumes the material does not change its structure in response to adsorbed gas, suggesting that flexible materials could still satisfy the DOE targets.

## INTRODUCTION

The transportation sector is dominantly powered by petroleum-based fuels [1]. Consequently, in the United States, it is responsible for 36% of energy-related carbon dioxide emissions [2] and  $\sim 50,000$  premature deaths per year associated with particulate matter and ozone emissions [3]. Natural gas and hydrogen ( $H_2$ ) are alternative transportation fuels that, if adopted widely, could mitigate climate change [4] and improve air quality for human health. More, the finite global petroleum resources are declining rapidly [5]. The development of technologies for the widespread adoption of sustainable transportation fuels, such as hydrogen, is therefore critical.

Natural gas, mostly methane, is considered a transition (to a renewable and clean) fuel because it emits 25% less carbon dioxide [6] and fewer toxic byproducts [7] upon combustion per unit energy produced compared to gasoline. From an economic standpoint, the supply of natural gas in the United States is increasing as a result of hydraulic fracturing and horizontal drilling techniques [8]. A positive environmental outlook for natural gas, however, is predicated on mitigating fugitive emissions (methane is itself a potent greenhouse gas) [9] and groundwater contamination [10] from hydraulic fracturing.

Hydrogen ( $H_2$ ) is the ultimate transportation fuel because it emits only water when it electrochemically reacts with oxygen in a fuel cell to power a vehicle. Notably, the environmental allure of hydrogen is predicated on its production via a renewable means, e.g. splitting wa-

ter using wind-generated electricity; currently, hydrogen ( $H_2$ ) is primarily produced by steam reforming of natural gas followed by the water-gas shift reaction, which emits carbon dioxide [11].

At ambient conditions, both methane and hydrogen gas possess a very low volumetric energy density compared to (liquid) gasoline. Consequently, under storage space constraints in passenger vehicles, natural gas and hydrogen must be densified for onboard storage to achieve a reasonable driving range on a “full” tank of fuel. Traditional densification approaches are liquefaction, at cryogenic temperatures and atmospheric pressure, or compression, at room temperature and high pressures. Both approaches require expensive infrastructure at refilling stations and significant energy input; e.g., the energy input to liquify hydrogen is  $\sim 30\%$  of its energy content [12]. Also, high-pressure storage tanks are heavy, thick-walled, and non-conformable, while cryogenic storage tanks are bulky, expensive, and afflicted by boil-off losses [13].

A promising approach to densify natural gas [14, 15] and hydrogen [16, 17] for vehicular storage at room temperature is through physical adsorption in nanoporous materials [18]. The internal surfaces of porous materials attract gas molecules through van der Waals, electrostatic, etc. interactions to achieve a higher adsorbed gas density than the bulk gas at the same temperature and pressure. Nanoporous materials could thus allow for room temperature and lower-pressure storage of natural gas and hydrogen and alleviate many drawbacks of high-pressure or low-temperature storage.

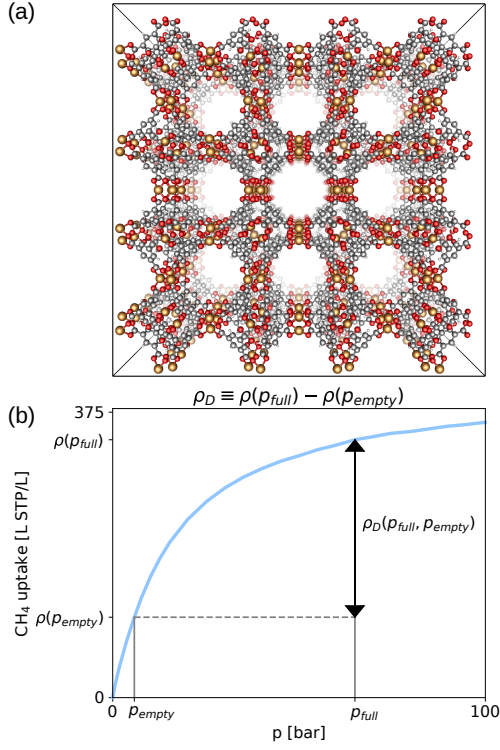


FIG. 1: Gas storage and delivery using metal-organic frameworks (MOFs). (a) the crystal structure of an archetype MOF, CuBTC [19]. (b) the methane adsorption isotherm in CuBTC [19] at 298 K (blue) (data from Ref. [15]). The deliverable capacity  $\rho_D$  is illustrated as the density of gas in the MOF at the storage pressure  $p_{full}$  minus the density at the discharge pressure  $p_{empty}$ .

For a vehicle employing a porous material to store natural gas or hydrogen, the (volumetric) *deliverable capacity* of the gas is the primary thermodynamic property that determines the driving range on a given “full” tank of fuel [15]. The adsorbed gas storage tank delivers the gaseous fuel to the engine via an (assumed) isothermal pressure swing [20]. The deliverable capacity (see Fig. 1b) is the density of the gas in the material at the storage pressure  $p_{full}$  minus the residual gas that remains adsorbed at the lowest pressure  $p_{empty}$  such that sufficient flow is maintained to feed the engine. For commercial feasibility, the US Department of Energy (DOE) has set deliverable capacity targets for both adsorbed methane and hydrogen storage and delivery for vehicles. For methane, the Advanced Research Projects Agency–Energy (ARPA-E) set a deliverable capacity target of 315 L STP  $\text{CH}_4$  per L of adsorbent at 298 K using a 65 bar to 5.8 bar pressure swing [21]. For hydrogen, the DOE set a series of progressive targets at five year intervals, with the ultimate target of 0.05 kg  $\text{H}_2/\text{L}$  [22] using a 100 bar to 5 bar pressure swing at a minimum of  $-40^\circ\text{C}$  [23]. Thus far,

despite the emergence of highly tunable materials with large surface areas, such as metal-organic frameworks [24] and covalent organic frameworks [25], no porous material has met these deliverable capacity targets.

To set realistic performance targets and optimally allocate resources to research efforts, in this work, we present a theoretical framework that places an intrinsic upper limit on the deliverable capacity of a pure gas in a rigid porous material and uses as input the experimentally measured properties of the bulk gas. Our extremum is provided by a substrate that offers a spatially uniform potential energy field felt by the gas. Applying our framework to methane and hydrogen gas, we find the US DOE deliverable capacity targets for natural gas and hydrogen storage and delivery are theoretically possible, but sufficiently close to the upper bound as to be impractical for any real, rigid porous material. Optimistically, new paradigms outside the scope of applicability of our theoretical framework, such as gas-induced structural transitions of the material, hold promise for meeting these targets, as evidenced by flexible MOF Co(bdp) which currently boasts the largest methane deliverable capacity [26].

## GAS STORAGE & DELIVERY BY ISOTHERMAL, PRESSURE-SWING ADSORPTION

Consider a pressure vessel onboard a vehicle (i.e. fuel tank) packed with porous material. At the filling stage, the tank is connected to a (pure) gaseous reservoir at pressure  $p_{full}$  and allowed to equilibrate. At this point, the adsorbed gas tank is considered full. While driving, gas desorbs from the adsorbent to the engine/fuel cell, driven by a pressure differential. The tank is considered depleted/empty when the pressure has dropped to  $p_{empty}$ , the pressure at which the flow rate of gas from the tank to the engine is insufficient. However, given  $p_{empty} \neq 0$  (pulling vacuum), residual gas will remain trapped in the adsorbent. Therefore, the driving range of the vehicle is primarily determined by the *deliverable capacity*  $\rho_D$  of the gas in the material (see Fig. 1b): the density of gas at  $p_{full}$  minus that at  $p_{empty}$ . The isothermal, volumetric deliverable capacity is an intrinsic property of the nanoporous material and its interaction with the gas.

## REVIEW OF PREVIOUS WORK

There has been considerable work attempting to establish an upper bound on the isothermal deliverable capacity in pressure-swing adsorption.

Early work showed that, in the simplified Langmuir model, there exists an optimal free energy of adsorp-

tion (which determines the Langmuir constant) that maximizes the deliverable capacity [27–29]. If the gas-substrate interaction is too weak (strong), too little (much) gas adsorbs (is retained) at  $p_{\text{full}}$  ( $p_{\text{empty}}$ ), diminishing the deliverable capacity. An upper bound on the deliverable capacity of a Langmuir material follows if each adsorption site is endowed with the optimal free energy of adsorption. However, remaining is the question of how many adsorption sites per volume a porous material can practically offer, under the constraint that these adsorption sites provide the optimal free energy of adsorption. Moreover, gas-gas attractions, neglected in the Langmuir model, could recruit more gas in the material at  $p_{\text{full}}$  than at  $p_{\text{empty}}$  and enhance the deliverable capacity [29].

Gómez-Gualdrón *et al.* [30] introduced a model that accounted for gas-gas interactions via an intermolecular potential and idealized the substrate in two different ways—as a: (1) set of discrete adsorption sites packed into an FCC lattice and (2) a volume endowed with a spatially uniform, background potential energy field. According to molecular simulation of methane adsorption, the ARPA-E deliverable capacity target of 315 L STP/L could be reached in both of these idealized substrates. However, both models (i) neglect the space occupied by atoms of the porous material that are needed to endow the adsorption sites/volume with the attractive potential energy and (ii) rely on a molecular model for methane.

A third body of work incorporated both gas-gas interactions *and* steric interactions of the gas with the atoms of the porous material. Simulations of methane adsorption in hundreds of thousands of explicit nanoporous crystal structures—both real and hypothetical—suggested that the ARPA-E deliverable capacity target is infeasible [21]; the highest simulated methane deliverable capacity was 196 cm<sup>3</sup> STP/cm<sup>3</sup>. Confidence in this conclusion rests upon (i) the accuracy of the intermolecular potentials describing the molecular interactions and (ii) the sufficient sampling of material space, i.e. that the structures considered are representative of the set of possible materials [31]. To further explore material space and address sensitivity to the intermolecular potentials: scaling the Lennard-Jones potential well depths of material atoms to model enhanced interactions [32], placing Lennard-Jones spheres in a unit cell randomly to form “pseudo-materials” [33], and generating fictitious potential energy fields via a generative adversarial network trained on zeolite structures [34] all generated model substrates that failed to meet the ARPA-E methane deliverable capacity target.

Finally, in a number of studies, molecular simulations of gas adsorption in a large pool of both existing and predicted nanoporous structures empirically shed light on performance limitations [21, 35–37]. Such studies can guide the development of new materials by allowing researchers to identify commonalities among materials that

have desirable properties. However, the largest observed simulated deliverable capacity among the pool of candidate materials in such studies is only a *lower bound* on the highest attainable deliverable capacity that is predicted upon the accuracy of the molecular models.

In this work, we place a rigorous upper bound on the isothermal deliverable capacity of a pure gas in a rigid substrate by endowing a control volume with a spatially uniform background energy field. Instead of using a molecular model for the gas [30], we use the experimental equation of state to account for gas-gas interactions. In addition, we prove using the calculus of variations that this spatially uniform substrate yields a maximal deliverable capacity. We use our framework to place an upper bound on the deliverable capacity of methane and hydrogen gas at conditions relevant to vehicular storage.

## METHODS

### An upper bound on the deliverable capacity

We now develop a thermodynamic framework that places an upper bound on the deliverable capacity of any pure gas in a rigid porous material.

The thermodynamic properties of a bulk, pure gas are characterized by an equation of state. Of particular interest for gas storage and delivery is the density of the gas  $\rho_g(\mu, T)$  as a function of chemical potential  $\mu$  and temperature  $T$ . We show  $\rho_g(\mu, T)$  for methane gas in Fig. 2 at  $T = 298$  K. For comparison, we also show the density of methane adsorbed into several porous materials.

To place an upper bound on the deliverable capacity, consider a substrate whose sole interaction with the gas is to introduce a spatially uniform potential energy  $\Phi$  for gas molecules in the control volume (where  $\Phi < 0$  for an attractive potential). Because this interaction is uniform within the substrate, the gas-gas interactions and thus fluid structure in such a substrate are identical to those of the pure gas at the same density and temperature. This allows us to obtain the adsorption properties of this model substrate using the experimentally measured properties of the pure gas [38]. Intuitively, the deliverable capacity of a gas in such a homogeneous substrate with the optimal potential energy is an upper bound because, in a real material, (i) spatial inhomogeneity of the potential energy results in some points in the control volume offering a suboptimal attraction for the gas and (ii) the atoms required to create the potential field exclude gas from occupying a fraction of the control volume and thus reduce utilized space.

The spatially uniform potential  $\Phi$  representing gas-substrate interactions behaves as an external potential and effectively shifts the chemical potential (or, equivalently, molar Gibbs free energy) of the gas in the material, just as gravitational potential energy causes the density

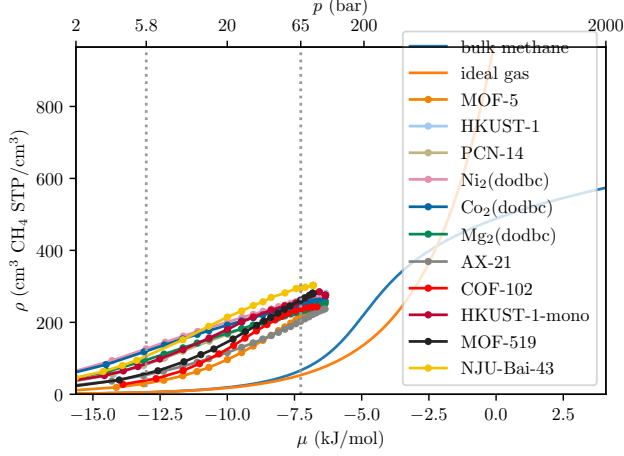


FIG. 2: The density of bulk methane, the ideal gas, and adsorbed gas in several porous materials at 298 K as a function of chemical potential (bottom axis) and pressure (top axis). The bulk methane density is from the National Institute of Standards and Technology (NIST) [38]. The methane adsorption isotherms in the porous materials are experimental data from Ref. [15, 39–42].

of air to vary with altitude. Consequently, the density of gas in our homogeneous substrate is:

$$\rho(\mu, T) = \rho_g(\mu - \Phi, T). \quad (1)$$

See Sec. for a derivation.

The deliverable capacity of gas in our homogeneous substrate is thus:

$$\begin{aligned} \rho_D(\Phi, T) &= \rho(\mu_{\text{full}}, T) - \rho(\mu_{\text{empty}}, T), \\ &= \rho_g(\mu_{\text{full}} - \Phi, T) - \rho_g(\mu_{\text{empty}} - \Phi, T), \end{aligned} \quad (2)$$

where  $\mu_{\text{full}}$  and  $\mu_{\text{empty}}$  are the chemical potentials corresponding to the pressures  $p_{\text{full}}$  and  $p_{\text{empty}}$ , respectively. Thus,  $\rho_D$  for our homogeneous substrate as a function of  $\Phi$  is the difference between two shifted versions of  $\rho_g(\mu; T)$ . Figure 3 shows the two shifted bulk methane density curves and their difference. The horizontal axis is the difference in molar Gibbs free energy of the gas, at fixed density (the density in the adsorbent) and temperature, between the gas within the substrate and the pure gas ( $\Delta g_{st}$ ), which is equal to  $\Phi$  in our model, but is pressure-dependent in a real crystal (see Sec. ). We see a potential  $\Phi$  that maximizes the deliverable capacity of our ideal substrate, balancing the need to maximize the density at  $p_{\text{full}}$  against the need to minimize residual gas retained at  $p_{\text{empty}}$ .

The optimal deliverable capacity of methane (298 K,  $p_{\text{full}} = 65$  bar,  $p_{\text{empty}} = 5.8$  bar) in our ideal, spatially uniform substrate is 374 L STP/L, achieved for  $\Phi_{\text{opt}} = 5.9$  kJ/mol.

An essential question is whether our idealized substrate, with spatially uniform potential  $\Phi_{\text{opt}}$  for the gas, places an upper bound on the deliverable capacity in all rigid porous materials. In Section , we show that our idealized substrate with spatially uniform potential  $\Phi_{\text{opt}}$  yields an *extremum* of the deliverable capacity over all possible *static potential energy fields*, provided the gas does not crystallize at the temperature and in the density range of interest. The potential energy field is *static* if it is unaffected by the presence of the gas; consequently, our model does not apply to flexible materials that undergo gas-induced conformation changes [43]. We next argue that this extremum is a maximum by addressing two alternative possibilities: the extremum could turn out to be (i) a saddle point or (ii) a local, rather than global, maximum.

Fig. 3 shows that  $\Phi_{\text{opt}}$  provides a maximum  $\rho_D$  over all *spatially uniform*, static potential energy fields. To qualitatively argue that the spatially uniform potential  $\Phi_{\text{opt}}$  provides a maximum deliverable capacity over *all* (including non-spatially uniform) static potential energy fields (a broader claim), consider a non-spatially-uniform variation on  $\Phi_{\text{opt}}$ . At low adsorbed gas densities, the lowest-energy positions will be preferentially occupied, while at higher densities, the additional gas molecules will be forced into higher energy locations. Thus, the mean attraction will be lowest at  $p_{\text{full}}$  and highest at  $p_{\text{empty}}$ . Therefore, the effect of a non-spatially uniform variation on  $\Phi_{\text{opt}}$  is to reduce the deliverable capacity. By the same argument,  $\Delta g_{st}$  increases monotonically with pressure. As shown in Sec. , this results in the deliverable capacity provided by a non-uniform potential with a given  $\Delta g_{st}$  at  $p_{\text{full}}$  or  $p_{\text{empty}}$  being lower than the deliverable capacity provided by a uniform potential with  $\Phi = \Delta g_{st}$ . Thus, a spatially uniform potential gives the maximal deliverable capacity amongst all static potential energy fields that give the same  $\Delta g_{st}$ , and the *optimal* uniform potential  $\Phi_{\text{opt}}$  will yield a greater deliverable capacity over any static, non-uniform potential.

### An external, spatially uniform potential $\Phi$ shifts the chemical potential $\mu$ of the gas

We show that imposing an external, spatially uniform potential  $\Phi$  to a gas has the effect of shifting the chemical potential  $\mu$  of the gas. Consider a control volume  $\Omega$  with volume  $V = |\Omega|$  (large enough to neglect boundary effects) that is endowed with the external, spatially uniform potential  $\Phi$ . Impose the grand-canonical ensemble, where this control volume can exchange energy and particles with a bath of gas at temperature  $T$  and chemical potential  $\mu$ .

To denote a microstate of this system, let  $N$  be the number of gas particles in the control volume and  $\mathbf{r}_1, \dots, \mathbf{r}_N$  be their positions. Then, the potential energy

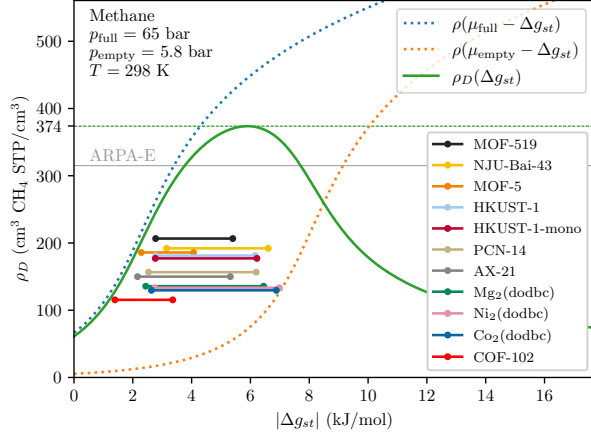


FIG. 3: The deliverable capacity of methane as a function of the attractive Gibbs free energy  $|\Delta g_{st}|$ . Experimental deliverable capacities for several porous materials (data from Ref. [15, 39–42]) are shown along with the experimental values for  $\Delta g_{st}$  at the empty and full pressures shown as dots connected by a line.

$E$  of a microstate of the control volume is:

$$E(\mathbf{r}_1, \dots, \mathbf{r}_N) = N\Phi + E_{gg}(\mathbf{r}_1, \dots, \mathbf{r}_N), \quad (4)$$

where  $E_{gg}$  is the (unknown and complicated) interatomic potential for gas-gas interactions that governs the (real) gas properties. The first term arises from each gas molecule experiencing the external potential  $\Phi$ , where  $\Phi < 0$  corresponds to attraction. To account for molecular rotational and vibrational degrees of freedom, we could treat the positions  $\mathbf{r}_i$  as the locations of atoms rather than molecules. In this case the gas-gas interactions will include both *intra-molecular* interactions and *inter-molecular* interactions.

The grand canonical partition function of the control volume is:

$$\Xi(\mu, V, T) = \sum_{N=0}^{\infty} \frac{1}{\Lambda^{3N} N!} \int_{\Omega} \dots \int_{\Omega} e^{-\beta E_{gg}(\mathbf{r}_1, \dots, \mathbf{r}_N)} e^{\beta(\mu - \Phi)N} d\mathbf{r}_1 \dots d\mathbf{r}_N.$$

We recognize this as the grand canonical partition function of the bulk gas in the control volume without the external potential, but shifted in chemical potential:

$$\Xi(\mu, V, T) = \Xi_g(\mu - \Phi, V, T) \quad (6)$$

where  $\Xi_g(\mu, V, T)$  is the grand partition function of the bulk gas in the control volume in the absence of an external potential. Importantly, this equivalency depends on the potential  $\Phi$  being spatially uniform. Therefore,

the thermodynamic properties of the gas atoms in the spatially uniform external potential  $\Phi$  (adsorbed in our idealized substrate) are equivalent to the properties of the bulk gas at chemical potential  $\mu - \Phi$  (where  $T$  is held fixed). As  $\Phi$  becomes more negative, corresponding to a more attractive adsorbent, the thermodynamic properties of the adsorbed gas in our ideal substrate are equivalent to the gas at a higher chemical potential.

### Proof of extremum

To show that a uniform potential gives the highest deliverable capacity, we consider an interaction potential between gas and substrate offering a potential energy field  $\Phi(\mathbf{r})$  that varies in space. We will show that the uniform potential has the highest deliverable capacity of the set of potentials having the same mean value, and to find the maximum deliverable capacity one maximizes over this mean value. In this proof, we make use of the Fourier transform of this potential:

$$\tilde{\Phi}(\mathbf{k}) \equiv \iiint \Phi(\mathbf{r}) e^{-i\mathbf{k} \cdot \mathbf{r}} d\mathbf{r} \quad (7)$$

The Fourier transform of a uniform potential is a Dirac delta function  $\tilde{\Phi}(\mathbf{k}) \propto \delta(\mathbf{k})$ . For a uniform potential to extremize the deliverable capacity, we must show that the functional derivative of the deliverable capacity with respect to  $\tilde{\Phi}(\mathbf{k})$  is zero for *nonzero* values of  $\mathbf{k}$ , i.e.

$$\frac{\delta \rho_D}{\delta \tilde{\Phi}(\mathbf{k})} = 0, \text{ if } \mathbf{k} \neq 0. \quad (8)$$

We note that this functional derivative may be non-zero for  $\mathbf{k} = 0$  because we separately maximize with respect to the mean value of the uniform potential  $\Phi$ . This means that

$$\frac{\delta N_{\text{full}}}{\delta \tilde{\Phi}(\mathbf{k})} = \frac{\delta N_{\text{empty}}}{\delta \tilde{\Phi}(\mathbf{k})} \quad (9)$$

where  $N_{\text{full}}$  and  $N_{\text{empty}}$  are the number of particles in the substrate at the full and empty pressure,  $p_{\text{full}}$  and  $p_{\text{empty}}$ , respectively.

Because the chemical potential  $\mu$  varies monotonically (5) with  $N$  at fixed temperature, we can consider how the chemical potential varies as we change  $\tilde{\Phi}(\mathbf{k})$  with the number of molecules held fixed. We demonstrate this using the cyclic chain rule, which shows us that

$$\left( \frac{\delta N}{\delta \tilde{\Phi}(\mathbf{k})} \right)_{\mu} = - \left( \frac{\delta \mu}{\delta \tilde{\Phi}(\mathbf{k})} \right)_N \left( \frac{\partial N}{\partial \mu} \right)_{\tilde{\Phi}(\mathbf{k})}. \quad (10)$$

Since changing the chemical potential changes the number of molecules in the general case, if we can show that  $\left( \frac{\delta \mu}{\delta \tilde{\Phi}(\mathbf{k})} \right)_N = 0$  then we will have shown that  $\left( \frac{\delta N}{\delta \tilde{\Phi}(\mathbf{k})} \right)_{\mu} =$



0. Thus we consider

$$\left( \frac{\delta \mu}{\delta \tilde{\Phi}(\mathbf{k})} \right)_N = \left( \frac{\delta \left( \frac{\partial F}{\partial N} \right)_V}{\delta \tilde{\Phi}(\mathbf{k})} \right)_N \quad (11)$$

$$= \left( \frac{\partial \left( \frac{\delta F}{\delta \tilde{\Phi}(\mathbf{k})} \right)_N}{\partial N} \right)_V \quad (12)$$

where we have made use of the derivative relationship between  $\mu$  and the Helmholtz free energy  $F$ , and have then reordered the functional and partial derivatives. Let us consider the interior derivative first. The derivative of the Helmholtz free energy with respect to the external potential  $\tilde{\Phi}(\mathbf{k})$  yields the number density:

$$\frac{\delta F}{\delta \tilde{\Phi}(\mathbf{k})} = \rho(\mathbf{k}) \quad (13)$$

The number density given a uniform potential is itself spatially uniform for any stable system in a fluid state at this density (i.e. does not spontaneously crystallize), and thus has a Fourier transform that is proportional to a Dirac  $\delta$ -function. Thus, the functional derivative  $\frac{\delta F}{\delta \tilde{\Phi}(\mathbf{r})}$  is actually a uniform function. We can insert this expression into Eq. 12 to find that

$$\left( \frac{\delta \mu}{\delta \tilde{\Phi}(\mathbf{k})} \right)_N \propto \delta(\mathbf{k}) \quad (14)$$

$$\left( \frac{\delta N}{\delta \tilde{\Phi}(\mathbf{k})} \right)_\mu \propto \delta(\mathbf{k}) \quad (15)$$

Thus, the functional derivative of both  $\mu$  and  $N$  with regard to  $\Phi(\mathbf{r})$  are themselves spatially uniform. Since we already maximize  $\rho_D$  with respect to the spatially uniform component of the potential (i.e.  $\mathbf{k} = 0$ ), the derivative of  $\rho_D$  with respect to any change of potential is zero.

This demonstrates that a spatially uniform potential leads to an extremum value of the deliverable capacity. This proof is insufficient, however, to show that it must be a true maximum.

#### The real-substrate analog of $\Phi$ is $\Delta g_{st}$

The parameter describing our idealized substrate is  $\Phi$ , the spatially uniform potential felt by a gas molecule adsorbed in the idealized substrate. A natural question is how this potential relates to the properties of real substrates. The effect of  $\Phi$  in our model is to shift the chemical potential  $\mu$  of the gas (see Sec. ). Because our ideal substrate shifts the chemical potential of the gas molecules by providing a spatially uniform potential energy field, the entropy of the gas in the ideal substrate is equal to the entropy of the gas in its bulk state at the

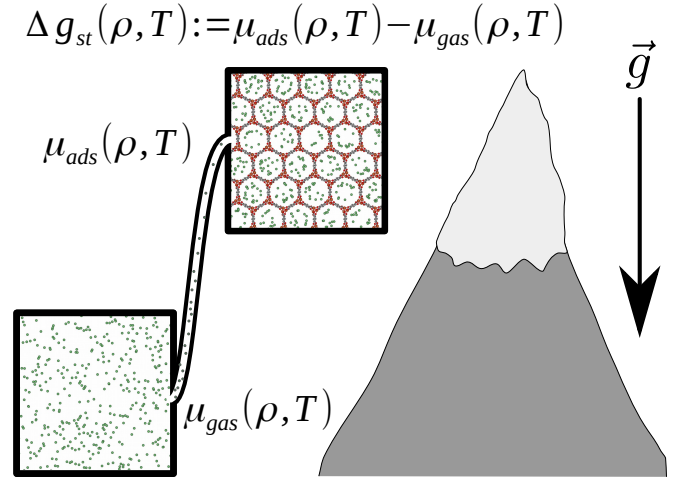


FIG. 4: An illustrative thought experiment to measure  $\Delta g_{st}$  by adjusting the altitude difference between two connected volumes, one free space and another containing a porous material.  $\Delta g_{st}$  is the difference in the gravitational potential energy when the density of gas in each volume is equal.

same density and temperature. In contrast, a real substrate provides a non-spatially uniform potential. Consequently, the entropy of the gas inside a real substrate is *not* equal to the entropy of the bulk gas at the same density and temperature. Therefore, the parameter analogous to  $\Phi$  in a real substrate will involve both energy and entropy. The real-substrate analog of  $\Phi$  is the shift of molar Gibbs free energy provided by the substrate, specifically an *isosteric* (or constant-density) shift of the Gibbs free energy:

$$\Delta g_{st}(\rho, T) \equiv \mu_{ads}(\rho, T) - \mu_{gas}(\rho, T). \quad (16)$$

The isosteric Gibbs free energy difference  $\Delta g_{st}$  is the difference in molar Gibbs free energy (equivalent to chemical potential) between the adsorbed gas system and the bulk gas *with the same density of gas molecules* and at the same temperature. The quantity  $\Delta g_{st}$  does *not* correspond to a change in the molar Gibbs free energy as a molecule is adsorbed, which is zero under conditions of coexistence. The quantity  $\Delta g_{st}$  in a real substrate is a direct analog to  $\Phi$  in our ideal substrate because it is the chemical potential shift needed to impose on the bulk gas in coexistence with the real substrate to achieve the same density as in the substrate (compare with eqn. 6). Figure 4 illustrates a hypothetical experiment to measure  $\Delta g_{st}$ . Two containers of equal volume are connected by a hose. One container holds the substrate, and the other is empty (apart from gas). The altitude of one container is adjusted until the number of gas molecules is equal in each container. The value of  $\Delta g_{st}$  is the gravitational potential energy difference of gas molecules in the two

boxes.

Note that  $\Delta g_{st}$  is a property of both the substrate and the identity of the gas. Because real substrates offer a *non*-spatially uniform potential,  $\Delta g_{st}(\rho, T)$  is a function of  $\rho$  and  $T$ , unlike our ideal, homogenous substrate where  $\Delta g_{st}(\rho, T) = \Phi$ . Consequently, throughout this article, we show  $\Delta g_{st}(\rho, T)$  for real substrates at both conditions relevant to gas storage and delivery,  $p_{\text{full}}$  and  $p_{\text{empty}}$ .

In practice, we can readily compute  $\Delta g_{st}(\rho, T)$  of a real gas/substrate system from (i) the (experimental or simulated) equilibrium adsorption isotherm of the gas in the substrate and (ii) the (experimental or simulated) chemical potential of the bulk gas. Consider the real substrate in thermodynamic equilibrium with a bulk gas at fixed temperature  $T$  and pressure  $p$ , and let  $\rho = \rho(p, T)$  be the density of gas in the substrate. At coexistence, the chemical potential of the bulk gas is equal to the chemical potential of the adsorbed gas in the substrate. Thus, we can use the experimentally known molar Gibbs free energy of the pure, bulk gas system at temperature  $T$  and pressure  $p$  to determine the molar Gibbs free energy of the adsorbed system:  $\mu_{\text{ads}}(\rho, T) = \mu_{\text{gas}}(p, T)$ . We can then also look up the known chemical potential of the bulk gas at the same density and temperature as in the substrate,  $\mu_{\text{gas}}(\rho, T)$ . Via eqn. 16,  $\Delta g_{st}$  follows from subtracting the two quantities.

An interesting question is how  $\Delta g_{st}$  relates to the commonly measured and reported isosteric heat of adsorption  $q_{st}$ , which is roughly the energy change when a gas molecule is adsorbed [44, 45]. Figure 5 shows how  $q_{st}$  compares to  $\Delta g_{st}$  for several prominent adsorbents. In every case,  $|q_{st}| > |\Delta g_{st}|$  because the gas in the adsorbent always has less entropy than the gas in the bulk at the same density and temperature. That is, while adsorption is energetically favored, it is entropically disfavored due to the restrictions imposed on the configuration of the gas molecules via steric interactions with the substrate itself; this counters the energetic attraction.

#### An upper bound when $\Delta g_{st}(\rho)$ is monotonic

Every adsorbent has a  $\Delta g_{st}$  at  $p_{\text{full}}$  and  $p_{\text{empty}}$  corresponding to a full and empty density,  $\rho_{\text{full}}$  and  $\rho_{\text{empty}}$ , respectively. The deliverable capacity of the adsorbent is equal to the difference between the full and empty density. Examining Fig. 6, we see that a significant variety of known experimental  $\Delta g_{st}$  curves are monotonic. Furthermore, our qualitative argument in Section suggests that this function *should* monotonically increase for rigid substrates, as increasing the density of gas causes some of the gas to reside in higher-energy sites. If this is always the case, the deliverable capacity of a real material (with a non-spatially uniform potential) with a given  $\Delta g_{st}$  at  $p_{\text{full}}$  or  $p_{\text{empty}}$  is bounded below by the deliverable capacity in our idealized substrate with  $\Phi = \Delta g_{st}$ , even for a

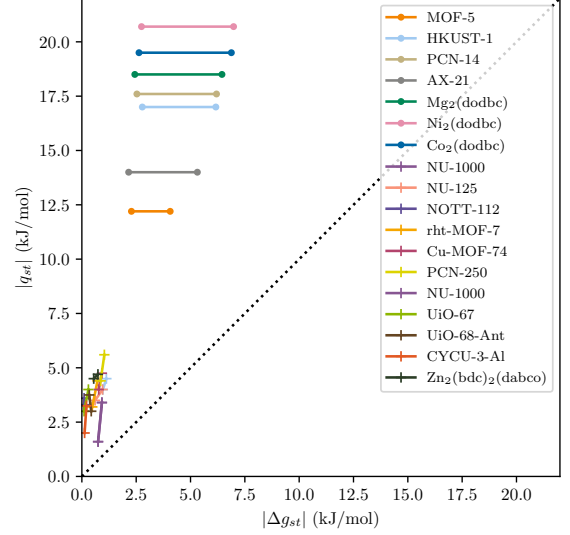


FIG. 5: Relationship between  $\Delta g_{st}$  and the isosteric heat  $q_{st}$  for several prominent adsorbents at room temperature (data from Ref. [15, 17]). The dots represent the properties of methane adsorption at 5.8 bar and 65 bar. The +’s represent the properties of hydrogen adsorption at 5 bar and 100 bar.

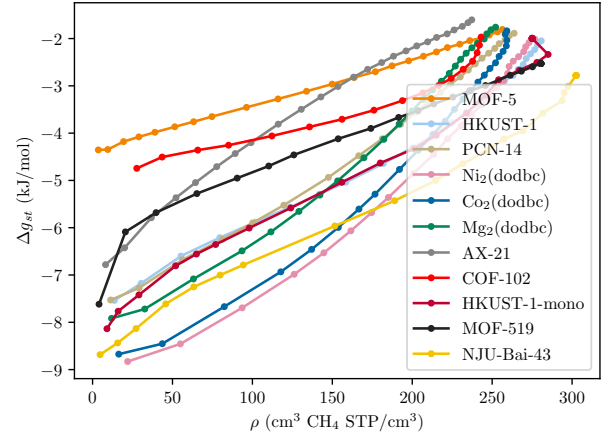


FIG. 6: The density-dependence of  $\Delta g_{st}$  of methane in several adsorbents (298 K). Note that  $\Delta g_{st}$  is monotonic in  $\rho$ . Data from Refs. [15, 39].

value of  $\Phi$  that is not optimal.

To show this, we perform a thought experiment illustrated in Fig. 7. We begin with two pairs of volumes. Two of these volumes contain a real adsorbent material. These adsorbent volumes are connected to bulk gas reservoirs at  $p_{\text{full}}$  and  $p_{\text{empty}}$  respectively, and by definition contain gas at density  $\rho_{\text{full}}$  and  $\rho_{\text{empty}}$ . The other two volumes contain gas at a density equal to the

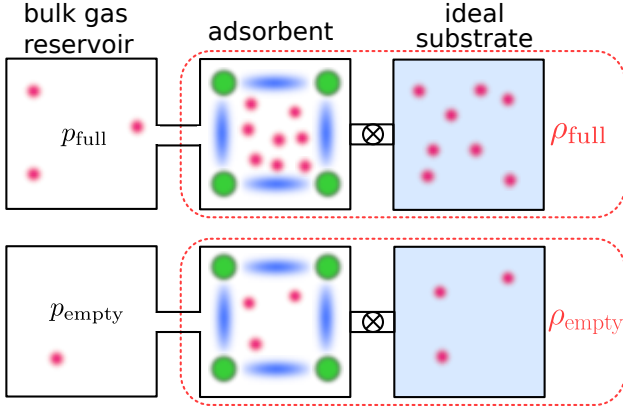


FIG. 7: A bulk gas reservoir is connected to a volume filled with adsorbent material (green/blue: material atoms, red: gas particles). The adsorbent is also connected, but with a closed valve, to an equal volume containing the ideal substrate (shaded blue background represents the uniform potential energy field  $\Phi$ ) with an equal density of gas as in the adsorbent. The top (bottom) shows a realization of this connected system where the pressure of the bulk gas is  $p_{\text{full}}$  ( $p_{\text{empty}}$ ), and thus the density of gas in the adsorbent is  $\rho_{\text{full}}$  ( $\rho_{\text{empty}}$ ) by definition. The deliverable capacity of the adsorbent is  $\rho_{\text{full}} - \rho_{\text{empty}}$ . We can determine if the deliverable capacity of gas in the ideal substrate is lower or higher than in the adsorbent by considering what happens when we open the valves connecting the two pairs of volumes containing adsorbent and the ideal substrate.

two adsorbent volumes ( $\rho_{\text{full}}$  and  $\rho_{\text{empty}}$ ), but contain our idealized substrate with uniform potential energy  $\Phi$ .

We now consider what happens if we open a diffusive connection between a volume of adsorbent and a volume with an idealized substrate that initially contain the same density of gas, for instance by connecting them with a tube. If the chemical potential in the idealized substrate is higher than in the porous material, then gas will flow out of the idealized substrate, lowering its density. Conversely, if the chemical potential is lower in the idealized substrate than in the volume of porous material, then gas will flow into the idealized substrate, increasing its density. The difference in chemical potential between those two volumes is

$$\Delta g_{st}(\rho) - \Phi = (\mu_{\text{ads}}(\rho) - \mu_{\text{gas}}(\rho)) - (\mu_{\Phi}(\rho) - \mu_{\text{gas}}(\rho)) \quad (17)$$

$$= \mu_{\text{ads}}(\rho) - \mu_{\Phi}(\rho). \quad (18)$$

where  $\mu_{\text{ads}}(\rho)$  and  $\mu_{\Phi}(\rho)$  are the chemical potentials of gas in the porous material and ideal substrate with potential  $\Phi$ , respectively. Thus if  $\Delta g_{st}(\rho_{\text{empty}}) = \Phi$ , the low-density containers will remain at their initial density after they are connected. Thus, the deliverable capacity of the adsorbent will be greater than the deliverable

capacity of the ideal substrate with uniform potential  $\Phi$  if and only if  $\Delta g_{st}(\rho_{\text{full}}) < \Phi$ , i.e. if  $\Delta g_{st}(\rho)$  does *not* monotonically increase, since then the gas in the high-density system will flow from the ideal substrate to the adsorbent. By the same token, if we consider the case where  $\Delta g_{st}(\rho_{\text{full}}) = \Phi$ , then for the adsorbent to achieve a greater deliverable capacity than the idealized substrate, the adsorbent must have less residual gas, which means that gas must spontaneously flow from the low-density adsorbent to the volume with potential  $\Phi$ , which means that  $\Delta g_{st}(\rho_{\text{empty}}) > \Phi$ . Once again, exceeding our upper bound requires a material with a  $\Delta g_{st}(\rho)$  that does not increase monotonically.

Taken together, this indicates that not only is our absolute upper bound an upper bound for rigid adsorbents, but the green curve labeled  $\rho_D(\Delta g_{st})$  in Figs. 3, 8, and 9 is an upper bound for materials with a non-optimal  $\Delta g_{st}$  at either  $p_{\text{full}}$  or  $p_{\text{empty}}$ .

## RESULTS

Although our theoretical framework allows us to place an upper bound on the deliverable capacity of many different gases in rigid porous materials, we focus on the maximal deliverable capacity of methane and hydrogen gas in our homogeneous substrate due to their application as transportation fuels. To characterize the density of the gases,  $\rho_g(p, T)$ , we use experimental data from NIST [38], which naturally includes quantum effects that particularly affect hydrogen at low temperature [46]. In the context of storage onboard passenger vehicles, we compare our upper bound with several prominent porous materials using experimental adsorption isotherms from the literature; we also compare with deliverable capacity targets set by the US DOE.

Figure 3 shows the upper bound for methane storage at room temperature ( $374 \text{ cm}^3 \text{ STP/cm}^3$ ). In addition to the predicted maximum deliverable capacity as a function of  $\Phi$ , the ARPA-E target of  $315 \text{ cm}^3 \text{ STP/cm}^3$  [47] is shown for context. For an adsorbent with at least 84% void fraction, the ARPA-E target is theoretically possible. The experimental deliverable capacities of several adsorbents [15] are also shown over a range of  $\Delta g_{st}$  (converted from the measured adsorption isotherm as explained in Sec. ). For context, the highest observed deliverable capacity for methane at room temperature in a rigid material is  $208 \text{ cm}^3 \text{ STP/cm}^3$  [21].

Storage of hydrogen is considerably more challenging owing to its relatively weak interaction with adsorbents. For room temperature storage, the DOE ULTIMATE deliverable capacity target [48] is within 6% of the upper bound. Figure 8 shows the theoretical upper bound curve for hydrogen storage along with experimental measurements for known adsorbents. The DOE ULTIMATE deliverable capacity target is theoretically possible, however



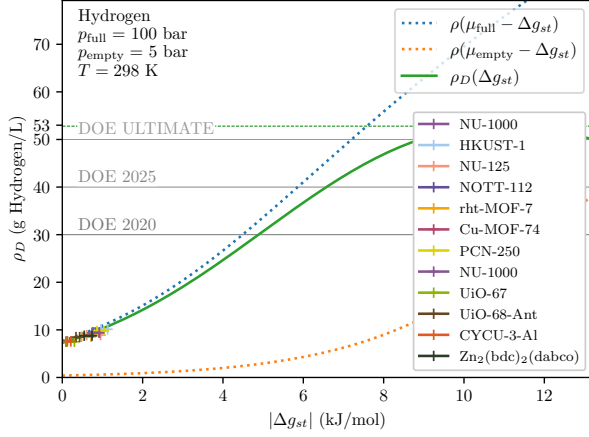


FIG. 8: Deliverable capacity of hydrogen at room temperature as a function of the attractive Gibbs free energy  $|\Delta g_{st}|$ . Experimental deliverable capacities for several porous materials (data from Ref. [17]) are shown along with the experimental values for  $\Delta g_{st}$  at the empty and full pressures shown as +’s connected by a line.

by such a small margin that we can safely rule out the possibility of reaching this target through storage and delivery of hydrogen in *any* rigid substrate at room temperature. Such a material would require a void fraction of at least 94%. On top of this, meeting the DOE ULTIMATE target requires an optimal  $|\Delta g_{st}|$  of 10 kJ/mol which is far greater than what is found in observed porous materials. This reflects the known fact that hydrogen interacts with substrates far more weakly than methane does. One approach to increase the deliverable capacity is to reduce the storage temperature. This is illustrated in Fig. 9, which shows the upper bound to the deliverable capacity of hydrogen at 77 K, the boiling point of nitrogen. The DOE ULTIMATE target in this case looks far more achievable, and with a much lower  $|\Delta g_{st}|$ . In fact, an empty tank at this temperature can satisfy the DOE 2020 target. The DOE ULTIMATE target is 14% below the upper bound. Actual adsorbents fall far short of the theoretical maximum.

Why do we not experimentally observe materials approaching the upper bound on the deliverable capacity? First and foremost, any adsorbent substrate will be composed of atoms, which will exclude the gas from some volume. Due to strong short-range interactions, from a longer length-scale perspective, substrate atoms must be approximately uniformly distributed to achieve strong attraction for gas atoms, imposing a limit on the pore volume. Second, in contrast to the homogeneous substrate, real materials have a spatially non-uniform attraction for gas atoms. As a result, there are regions of space with non-optimal attraction. For hydrogen, there is the fur-

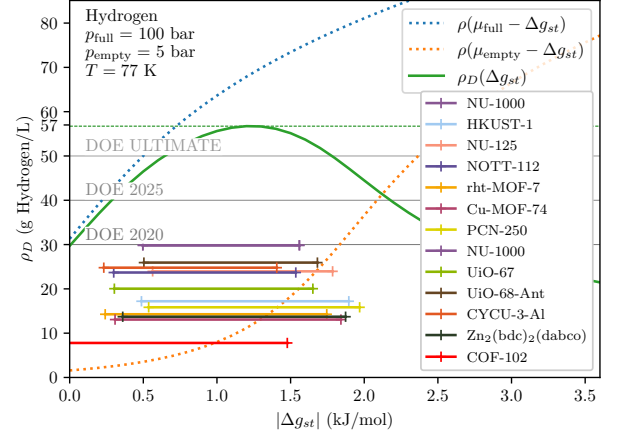


FIG. 9: Deliverable capacity of hydrogen at 77 K as a function of the attractive Gibbs free energy  $\Delta g_{st}$ . Experimental deliverable capacities for several porous materials (data from Ref. [17, 39]) are shown along with the experimental values for  $\Delta g_{st}$  at the empty and full pressures shown as +’s connected by a line.

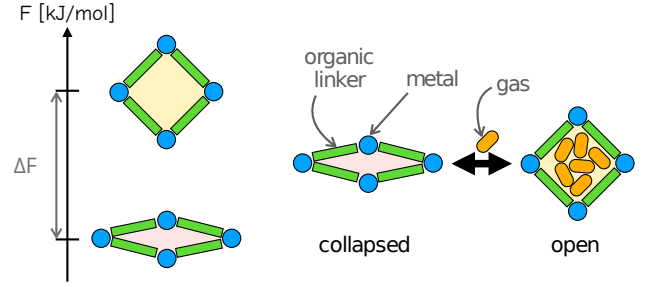


FIG. 10: Cartoon of a two-phase, collapsing material. The material can exist in two phases: an open phase in which gas molecules can adsorb, and a closed phase that is collapsed and cannot fit any gas molecules. Take the closed phase as more stable, so that the material can collapse and expel residual gas. The pressure of gas at which the structural transition occurs depends on the gas-host interactions and relative stability of the phases. We wish for the structural transition to occur between  $p_{full}$  and  $p_{empty}$ .

ther issue that there are no known *physical* interactions that are sufficiently strong to give an optimal deliverable capacity at room temperature.

## FLEXIBLE TWO-PHASE MODEL

While our deliverable capacity limit does not apply to materials that change conformation in response to gas adsorption, here we adapt our theoretical framework to pertain to bistable adsorbents modeled after Co(bdp) [26].

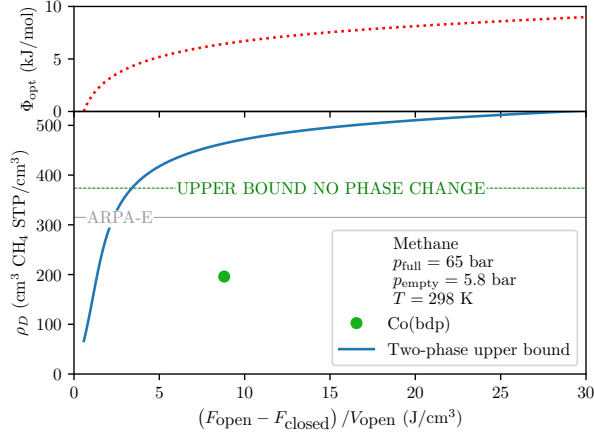


FIG. 11: Maximal possible deliverable capacity of methane in a two-phase, collapsing substrate at 298 K as a function of the free energy difference between open and closed phases. The experimental deliverable capacity for Co(bdp) is shown for comparison, along with the free energy difference between open and closed conformations [26].

Actuated by the presence of gas, Co(bdp) can switch between two distinct structural phases: an “open” phase where gas molecules can fit in the pore space and a collapsed, “closed” phase in which no gas can fit inside.

We follow Coudert *et al.* [49] in developing a thermodynamic model for a two-phase, collapsing adsorbent like Co(bdp). Let  $\Delta F = F_{\text{open}} - F_{\text{closed}}$  be the Helmholtz free energy difference per mole of adsorbent between the two phases in the absence of gas. Suppose the closed phase is more stable ( $\Rightarrow \Delta F > 0$ ), so that upon a reduction in the pressure of the gas, the material can collapse and expel all residual gas to enhance the deliverable capacity compared to rigid materials that will retain some gas at  $p_{\text{empty}}$ . In addition, assume the open phase hosts a uniform, attractive potential energy field  $\Phi < 0$  for gas molecules to adsorb, so that eqn. 6 holds for the material when in the open phase.

This model of a two-phase, collapsing material has no upper bound on the deliverable capacity, since  $|\Phi|$  and  $\Delta F$  can together be increased without bound. We can, however, place a bound on the deliverable capacity for a fixed  $\Delta F$ , since if the gas is too strongly attracted to the open phase, the material will remain open at  $p_{\text{empty}}$ , and, then, our rigid upper bound applies. We place an upper bound on the deliverable capacity in the two-phase material by identifying the attractive interaction  $\Phi$  that balances the gas-host attractions in the idealized-open-substrate at  $p_{\text{empty}}$  with the free energy penalty to open.

For an enhancement of the deliverable capacity by this two-phase, flexible material, the open phase must be preferred at  $p_{\text{full}}$ , with the closed phase preferred at  $p_{\text{empty}}$ .

The upper bound for the two-phase material is found by identifying the largest possible attraction  $|\Phi|$  consistent with the material transitioning between  $p_{\text{empty}}$  and  $p_{\text{full}}$  to expel all residual gas. The material changes phases when the osmotic potentials of the open and closed systems with and without gas, respectively, are equal [49] (neglecting any hysteresis). Thus, the optimal background potential  $\Phi_{\text{opt}}$  equates the grand potential of the gas in the open phase with the free energy difference between the two phases at  $p_{\text{empty}}$ :

$$\frac{\Delta F}{V_{\text{open}}} = \int_{-\infty}^{\mu_{\text{empty}}} \rho_g(\mu - \Phi_{\text{opt}}) d\mu, \quad (19)$$

where we follow Coudert *et al.* [49] and neglect the  $pV$  terms, and  $V_{\text{open}}$  is the molar volume of the open phase. I.e.,  $|\Phi_{\text{opt}}|$  gives the maximal gas-open-host attractions under the constraint that the material collapses and expels all residual gas at  $p_{\text{empty}}$ ; if the attraction were greater, the material would refuse to collapse and expel its gas at  $p_{\text{full}}$ . The deliverable capacity is then the density of gas in the open phase at  $p_{\text{full}}$ ,  $\rho_g(\mu_{\text{full}} - \Phi_{\text{opt}}, T)$  with  $\Phi_{\text{opt}}$  satisfying eqn. 19.

Figure 11 illustrates how the upper bound on the deliverable capacity of methane in a two-phase, collapsing material depends on  $\Delta F$ — and the  $\Phi_{\text{opt}}$  that maximizes the deliverable capacity. For comparison, we include the free energy difference for Co(bdp) [50] and its measured deliverable capacity. Indeed, the deliverable capacity of a two-phase, collapsing material can exceed that of a rigid material if (i) the closed phase is sufficiently stable relative to the open phase and (ii) the gas has a correspondingly high affinity for the open phase. Figure 12 shows the corresponding result for hydrogen storage, indicating that, for a flexible material to reach the DOE ULTIMATE deliverable capacity, it would require far greater stability for the closed phase, as well as an unprecedented level of attractive interaction for hydrogen.

## CONCLUSIONS

We have established an upper bound on the deliverable capacity via pressure-swing adsorption in rigid porous solids based on experimentally measured properties of pure gases. While these upper bounds do not rule out the discovery of materials that reach current DOE targets for room temperature hydrogen and methane storage, they cast strong doubt on the possibility of achieving these goals when we consider the additional constraints imposed due to steric hindrance between substrate atoms and the adsorbate. Our upper bound does indicate that those goals cannot be exceeded by more than 16% for methane and 6% for hydrogen. Fortunately, there are some limitations to these upper bounds which suggest avenues for future developments.

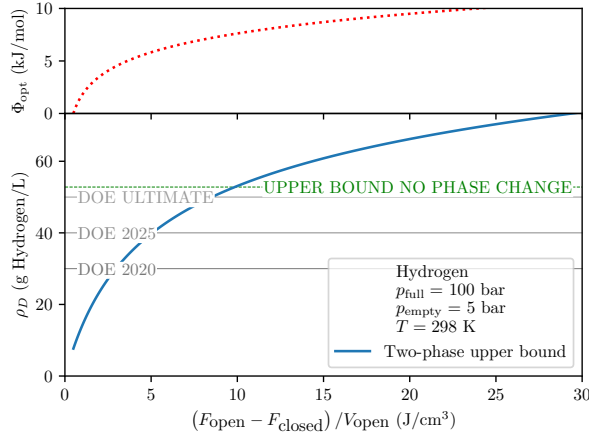


FIG. 12: Deliverable capacity of hydrogen in a flexible, two-phase substrate at 298 K as a function of the free energy difference between open and closed phases.

The first limitation of our proof is that we restricted ourselves to *isothermal* pressure swing storage (which is consistent with the targets set by DOE). By raising the temperature of the adsorbent during gas discharge to drive off residual gas [32], the deliverable capacity could be enhanced, albeit at the cost of a more complicated engineering design of the fuel tank and vehicle. We cannot place an upper bound on such a process using our approach because, with changing temperature, a uniform potential may not give the maximum deliverable capacity. A nonuniform potential will lower the entropy of the adsorbed gas, which will make the gas easier to release by raising the temperature.

The second limitation of our proof arises in the assumption of a rigid substrate. The rigid substrate acts as a static potential energy field for gas molecules that is unchanged by the adsorption of gas. For most porous materials this is a reasonable approximation, and this assumption is frequently made in both the simulation and theory of porous materials [51]. However, there are cases where the substrate can provide a very strong gas-density-dependent interaction through structural flexibility [43]. A flagship example is MOF Co(bdp) [50], which possesses a wine-rack-like topology capable of hinge motion. At low methane pressure, Co(bdp) adopts a collapsed, nonporous state, but expands to a porous state and fills with gas at higher pressures [26]. This allows Co(bdp) to fully expel its residual gas at low pressures. Flexible materials could have significantly higher deliverable capacities, as we have shown for two-phase structures that collapse and expel all residual gas at low pressures.

Several studies elucidated relationships between structural features of nanoporous materials—such as void fraction, pore size, and surface area—and their deliverable

capacity of various gases [21, 32, 37, 52, 53]. Such structure-property relationships serve as useful heuristics for designing new materials with high deliverable capacity. However, the intention of our paper is not to discover structure-property relationships. Rather, we place our upper bound on the deliverable capacity of [rigid] materials that holds irrespective of how the structural features of the material are tuned.

For vehicular gas storage, gravimetric deliverable capacity (amount of gas per mass of material) may be considered as a material performance metric to avoid a heavy adsorbed-gas fuel tank. However, the volumetric deliverable capacity (amount of gas per volume of material) dominantly determines the driving range on a full fuel tank of a given volume [15]. That said, several articles have explored the tradeoff between gravimetric and volumetric deliverable capacity, particularly for hydrogen storage [36, 54–56].

We note that our upper bound can readily be applied to the storage of other gasses of interest, with the proviso that the gas is far from crystallization. Our code is available at <https://github.com/droundy/thesis-pommerenck/tree/master/gas-adsorption>.

- 
- [1] S. C. Davis, S. W. Diegel, and R. G. Boundy, *Transportation energy data book*, Tech. Rep. (Oak Ridge National Laboratory, 2009).
  - [2] U. E. I. Administration, What are u.s. energy-related carbon dioxide emissions by source and sector?, <https://www.eia.gov/tools/faqs/faq.php?id=75&t=11> (2018).
  - [3] F. Caiazzo, A. Ashok, I. A. Waitz, S. H. Yim, and S. R. Barrett, Air pollution and early deaths in the united states. part i: Quantifying the impact of major sectors in 2005, *Atmospheric Environment* **79**, 198 (2013).
  - [4] C. McGlade and P. Ekins, The geographical distribution of fossil fuels unused when limiting global warming to 2 °c, *Nature* **517**, 187 (2015).
  - [5] S. Sorrell, J. Speirs, R. Bentley, A. Brandt, and R. Miller, Global oil depletion: A review of the evidence, *Energy Policy* **38**, 5290 (2010).
  - [6] U. Energy Information Administration, How much carbon dioxide is produced when different fuels are burned? (2018).
  - [7] M. Q. Wang and H. S. Huang, *A full fuel-cycle analysis of energy and emissions impacts of transportation fuels produced from natural gas*, Tech. Rep. (Argonne National Lab., IL (US), 2000).
  - [8] U. E. I. Administration, Natural gas explained: Where our natural gas comes from, <https://www.eia.gov/energyexplained/natural-gas/where-our-natural-gas-comes-from.php> (2019).
  - [9] R. A. Alvarez, S. W. Pacala, J. J. Winebrake, W. L. Chameides, and S. P. Hamburg, Greater focus needed on methane leakage from natural gas infrastructure, *Proceedings of the National Academy of Sciences* **109**, 6435 (2012), <https://www.pnas.org/content/109/17/6435.full.pdf>.

- [10] S. G. Osborn, A. Vengosh, N. R. Warner, and R. B. Jackson, Methane contamination of drinking water accompanying gas-well drilling and hydraulic fracturing, *proceedings of the National Academy of Sciences* **108**, 8172 (2011).
- [11] G. W. Crabtree, M. S. Dresselhaus, and M. V. Buchanan, The hydrogen economy, *Physics Today* **57**, 39 (2004).
- [12] U. Bossel and B. Eliasson, Energy and the hydrogen economy, *Alternative Fuels Data Center*, US DOE (2003).
- [13] M. F. Hasan, A. M. Zheng, and I. Karimi, Minimizing boil-off losses in liquefied natural gas transportation, *Industrial & Engineering Chemistry Research* **48**, 9571 (2009).
- [14] T. A. Makal, J.-R. Li, W. Lu, and H.-C. Zhou, Methane storage in advanced porous materials, *Chemical Society Reviews* **41**, 7761 (2012).
- [15] J. A. Mason, M. Veenstra, and J. R. Long, Evaluating metal-organic frameworks for natural gas storage, *Chemical Science* **5**, 32 (2014).
- [16] M. P. Suh, H. J. Park, T. K. Prasad, and D.-W. Lim, Hydrogen storage in metal-organic frameworks, *Chemical Reviews* **112**, 782 (2011).
- [17] P. García-Holley, B. Schweitzer, T. Islamoglu, Y. Liu, L. Lin, S. Rodriguez, M. H. Weston, J. T. Hupp, D. A. Gómez-Gualdrón, T. Yildirim, *et al.*, Benchmark study of hydrogen storage in metal-organic frameworks under temperature and pressure swing conditions, *ACS Energy Letters* **3**, 748 (2018).
- [18] A. Schoedel, Z. Ji, and O. M. Yaghi, The role of metal-organic frameworks in a carbon-neutral energy cycle, *Nature Energy* **1**, 16034 (2016).
- [19] S. S.-Y. Chui, S. M.-F. Lo, J. P. Charmant, A. G. Orpen, and I. D. Williams, A chemically functionalizable nanoporous material  $[\text{Cu}_3(\text{tma})_2(\text{H}_2\text{O})_3]_n$ , *Science* **283**, 1148 (1999).
- [20] S. Sircar, Pressure swing adsorption, *Industrial & engineering chemistry research* **41**, 1389 (2002).
- [21] C. M. Simon, J. Kim, D. A. Gómez-Gualdrón, J. S. Camp, Y. G. Chung, R. L. Martin, R. Mercado, M. W. Deem, D. Gunter, M. Haranczyk, D. S. Sholl, R. Q. Snurr, and B. Smit, The materials genome in action: identifying the performance limits for methane storage, *Energy & Environmental Science* **8**, 1190 (2015).
- [22] D. O. of ENERGY EFFICIENCY & RENEWABLE ENERGY, Doe technical targets for onboard hydrogen storage for light-duty vehicles (2019).
- [23] M. D. Allendorf, Z. Hulvey, T. Gennett, A. Ahmed, T. Autrey, J. Camp, E. S. Cho, H. Furukawa, M. Haranczyk, M. Head-Gordon, *et al.*, An assessment of strategies for the development of solid-state adsorbents for vehicular hydrogen storage, *Energy & Environmental Science* **11**, 2784 (2018).
- [24] H. Furukawa, K. E. Cordova, M. O’Keeffe, and O. M. Yaghi, The chemistry and applications of metal-organic frameworks, *Science* **341**, 1230444 (2013).
- [25] C. S. Diercks and O. M. Yaghi, The atom, the molecule, and the covalent organic framework, *Science* **355**, 923 (2017).
- [26] J. A. Mason, J. Oktawiec, M. K. Taylor, M. R. Hudson, J. Rodriguez, J. E. Bachman, M. I. Gonzalez, A. Cervellino, A. Guagliardi, C. M. Brown, P. Llewellyn, N. Masciocchi, and J. Long, Methane storage in flexible metal-organic frameworks with intrinsic thermal management, *Nature* **527**, 357 (2015).
- [27] K. R. Matranga, A. L. Myers, and E. D. Glandt, Storage of natural gas by adsorption on activated carbon, *Chemical Engineering Science* **47**, 1569 (1992).
- [28] S. K. Bhatia and A. L. Myers, Optimum conditions for adsorptive storage, *Langmuir* **22**, 1688 (2006).
- [29] C. M. Simon, J. Kim, L.-C. Lin, R. L. Martin, M. Haranczyk, and B. Smit, Optimizing nanoporous materials for gas storage, *Physical Chemistry Chemical Physics* **16**, 5499 (2014).
- [30] D. A. Gómez-Gualdrón, C. M. Simon, W. Lassman, D. Chen, R. L. Martin, M. Haranczyk, O. K. Farha, B. Smit, and R. Q. Snurr, Impact of the strength and spatial distribution of adsorption sites on methane deliverable capacity in nanoporous materials, *Chemical Engineering Science* **159**, 18 (2017).
- [31] S. M. Moosavi, A. Nandy, K. M. Jablonka, D. Ongari, J. P. Janet, P. G. Boyd, Y. Lee, B. Smit, and H. J. Kulik, Understanding the diversity of the metal-organic framework ecosystem, *Nature communications* **11**, 1 (2020).
- [32] D. A. Gómez-Gualdrón, C. E. Wilmer, O. K. Farha, J. T. Hupp, and R. Q. Snurr, Exploring the limits of methane storage and delivery in nanoporous materials, *The Journal of Physical Chemistry C* **118**, 6941 (2014).
- [33] A. R. Kaija and C. E. Wilmer, High-pressure methane adsorption in porous lennard-jones crystals, *The Journal of Physical Chemistry Letters* **9**, 4275 (2018).
- [34] S. Lee, B. Kim, and J. Kim, Predicting performance limits of methane gas storage in zeolites with an artificial neural network, *Journal of Materials Chemistry A* **7**, 2709 (2019).
- [35] L. Firlej, P. Pfeifer, and B. Kuchta, Understanding universal adsorption limits for hydrogen storage in nanoporous systems, *Advanced Materials* **25**, 5971 (2013).
- [36] J. Goldsmith, A. G. Wong-Foy, M. J. Cafarella, and D. J. Siegel, Theoretical limits of hydrogen storage in metal-organic frameworks: opportunities and trade-offs, *Chemistry of Materials* **25**, 3373 (2013).
- [37] A. Ahmed, S. Seth, J. Purewal, A. G. Wong-Foy, M. Veenstra, A. J. Matzger, and D. J. Siegel, Exceptional hydrogen storage achieved by screening nearly half a million metal-organic frameworks, *Nature communications* **10**, 1 (2019).
- [38] E. Lemmon, M. McLinden, and D. Friend, NIST Chemistry WebBook, NIST Standard Reference Database Number 69 (National Institute of Standards and Technology, Gaithersburg MD, 20899, retrieved 2019) Chap. Thermophysical Properties of Fluid Systems, <http://webbook.nist.gov>.
- [39] H. Furukawa and O. M. Yaghi, Storage of hydrogen, methane, and carbon dioxide in highly porous covalent organic frameworks for clean energy applications, *Journal of the American Chemical Society* **131**, 8875 (2009).
- [40] T. Tian, Z. Zeng, D. Vulpe, M. E. Casco, G. Divitini, P. A. Midgley, J. Silvestre-Albero, J.-C. Tan, P. Z. Moghadam, and D. Fairen-Jimenez, A sol-gel monolithic metal-organic framework with enhanced methane uptake, *Nature materials* **17**, 174 (2018).
- [41] F. Gándara, H. Furukawa, S. Lee, and O. M. Yaghi, High methane storage capacity in aluminum metal-organic frameworks, *Journal of the American Chemical Society* **136**, 5271 (2014).
- [42] M. Zhang, W. Zhou, T. Pham, K. A. Forrest, W. Liu, Y. He, H. Wu, T. Yildirim, B. Chen, B. Space, *et al.*, Fine tuning of mof-505 analogues to reduce low-pressure

- methane uptake and enhance methane working capacity, *Angewandte Chemie* **129**, 11584 (2017).
- [43] A. Schneemann, V. Bon, I. Schwedler, I. Senkovska, S. Kaskel, and R. A. Fischer, Flexible metal–organic frameworks, *Chemical Society Reviews* **43**, 6062 (2014).
- [44] S. Sircar, R. Mohr, C. Ristic, and M. Rao, Isosteric heat of adsorption: theory and experiment, *The Journal of Physical Chemistry B* **103**, 6539 (1999).
- [45] Y. Tian and J. Wu, Differential heat of adsorption and isosteres, *Langmuir* **33**, 996 (2017).
- [46] A. A. Kumar, H. Jobic, and S. K. Bhatia, Quantum effects on adsorption and diffusion of hydrogen and deuterium in microporous materials, *The Journal of Physical Chemistry B* **110**, 16666 (2006).
- [47] A. R. P. A.-E. (ARPA-E), Move (methane opportunities for vehicular energy) program overview, [https://arpa-e.energy.gov/sites/default/files/documents/files/MOVE\\_ProgramOverview.pdf](https://arpa-e.energy.gov/sites/default/files/documents/files/MOVE_ProgramOverview.pdf) (2012).
- [48] DOE. Multi-Year Research, Development, and Demonstration Plan (U.S. Department of Energy (DOE): Washington, DC, retrieved 2019).
- [49] F.-X. Coudert, M. Jeffroy, A. H. Fuchs, A. Boutin, and C. Mellot-Draznieks, Thermodynamics of guest-induced structural transitions in hybrid organic- inorganic frameworks, *Journal of the American Chemical Society* **130**, 14294 (2008).
- [50] H. J. Choi, M. Dinca, and J. R. Long, Broadly hysteretic h<sub>2</sub> adsorption in the microporous metal- organic framework co (1, 4-benzenedipyrazolate), *Journal of the American Chemical Society* **130**, 7848 (2008).
- [51] T. Düren, Y.-S. Bae, and R. Q. Snurr, Using molecular simulation to characterise metal–organic frameworks for adsorption applications, *Chemical Society Reviews* **38**, 1237 (2009).
- [52] P. Z. Moghadam, T. Islamoglu, S. Goswami, J. Exley, M. Fantham, C. F. Kaminski, R. Q. Snurr, O. K. Farha, and D. Fairen-Jimenez, Computer-aided discovery of a metal–organic framework with superior oxygen uptake, *Nature communications* **9**, 1 (2018).
- [53] M. Tong, Y. Lan, Z. Qin, and C. Zhong, Computation-ready, experimental covalent organic framework for methane delivery: Screening and material design, *The Journal of Physical Chemistry C* **122**, 13009 (2018).
- [54] D. A. Gómez-Gualdrón, T. C. Wang, P. García-Holley, R. M. Sawelewa, E. Argueta, R. Q. Snurr, J. T. Hupp, T. Yildirim, and O. K. Farha, Understanding volumetric and gravimetric hydrogen adsorption trade-off in metal–organic frameworks, *ACS applied materials & interfaces* **9**, 33419 (2017).
- [55] Z. Chen, P. Li, R. Anderson, X. Wang, X. Zhang, L. Robison, L. R. Redfern, S. Moribe, T. Islamoglu, D. A. Gómez-Gualdrón, *et al.*, Balancing volumetric and gravimetric uptake in highly porous materials for clean energy, *Science* **368**, 297 (2020).
- [56] A. Ahmed and D. J. Siegel, Predicting hydrogen storage in mofs via machine learning, *Patterns* **2**, 100291 (2021).